Electro-osmotic instability of concentration enrichment in curved geometries for an aqueous electrolyte

Bingrui Xu,[1,*] Zhibo Gu,[1,*] Wei Liu [],[2] Peng Huo,[1] Yueting Zhou,[2] S. M. Rubinstein [],[3]
M. Z. Bazant [],[4] B. Zaltzman,[5] I. Rubinstein [],[5] and Daosheng Deng [][1,†]

[1]*Department of Aeronautics and Astronautics, Fudan University, Shanghai 200433, China*
[2]*School of Aerospace Engineering and Applied Mechanics, Tongji University, Shanghai 200092, China*
[3]*John A. Paulson School of Engineering and Applied Sciences, Harvard University, Cambridge,
Massachusetts 02138, USA*
[4]*Department of Chemical Engineering and Department of Mathematics, Massachusetts Institute of
Technology, Cambridge, Massachusetts 02139, USA*
[5]*Department of Mathematics and the BIDR, Ben-Gurion University of the Negev, Sede Boqer Campus, Sede
Boqer 8499000, Israel*

We report that an electro-osmotic instability of concentration enrichment in curved geometries for an aqueous electrolyte, as opposed to the well-known one, is initiated exclusively at the enriched interface (anode), rather than at the depleted one (cathode). For this instability, the limitation of an unrealistically high material Peclet number in planar geometry is eliminated by the strong electric field arising from the line charge singularity. In a model setup of concentric circular electrodes, we show by stability analysis, numerical simulation, and experimental visualization that instability occurs at the inner anode, below a critical radius of curvature. The stability criterion is also formulated in terms of a critical electric field and extended to arbitrary (two-dimensional) geometries by conformal mapping. This discovery suggests that transport may be enhanced in processes limited by salt enrichment, such as reverse osmosis, by triggering this instability with needlelike electrodes.

Ion transport through an aqueous electrolyte plays an essential role in numerous electrochemical technologies, such as fuel cells, flow batteries, electrodialysis, and capacitive deionization for water desalination [1,2]. Under applied DC current or voltage, due to the electromigration and diffusion, ions are redistributed spatially to produce concentration polarization, i.e., the regions of concentration depletion and enrichment. As the concentration near an ion-selective interface (the membrane, electrode, or nanochannel) becomes strongly depleted by diffusion limitation, the current as a function of voltage tends to saturate at the limiting value, followed by the region of overlimiting conductance.

Several mechanisms for this have been discussed [3,4]. In bulk liquid electrolytes, the main physical mechanism for overlimiting current likely is nonequilibrium electro-osmotic instability (NE-EOI) [5–9]. NE-EOI relies on the transformation of the electric double layer on the electrode or membrane causing salt depletion from its typical nanoscale quasiequilibrium structure to a nonequilibrium structure of extended space charge [5,6]. During NE-EOI, overlimiting current

---

*These authors contributed equally to this work.
†dsdeng@fudan.edu.cn

is sustained by vortical flows at a macroscopic scale ($100~\mu$m) in the depleted region, which have been shown to result from instability in parallel-plate (one-dimensional) geometries, or in a threshold-less manner in systems with a broken symmetry [7–9]. In confined systems, new transport mechanisms can arise. In particular, overlimiting current can be sustained by surface conduction or electro-osmotic flow along the confining surfaces in microchannels [10–13] or porous media [14–18].

Recently, equilibrium electro-osmotic instability has been invoked as a possible mechanism of the overlimiting current by relaxing the perfect charge selectivity or infinite conductivity assumptions [19,20]. In principle, equilibrium electrokinetic instability in a perfect plane-parallel electrochemical cell has been ruled out, since the required minimal material Peclet number ($\text{Pe}_{\min} = 8$) is about one order of magnitude higher than that of the typical aqueous electrolyte solution ($\text{Pe}_{\text{aqu}} \simeq 0.5$) [21,22]. Physically, for quasiequilibrium electric double layer, the limiting electro-osmotic slip velocity is proportional to the tangential concentration gradient [6]. In the concentration depletion region near the interface (such as the cathode), a seeding vortex is suppressed by a negative feedback, since the descending portion of the vortex towards interface brings the high bulk concentration to the cathode. In the concentration enrichment region, the opposite is true, making the instability possible, if only the material Peclet number were an order of magnitude larger.

In this Rapid Communication, we demonstrate that equilibrium electrokinetic instability can indeed appear exclusively in the region of *concentration enrichment* for an aqueous solution, by eliminating the limitation of unrealistically high Pe in planar geometry via the strong electric field due to the singularity of line charges. This electro-osmotic instability of concentration enrichment (EOI-CE) is different from all the previously studied nonequilibrium or equilibrium EOI occurring in the depletion region. We predict EOI-CE by numerical simulation and by extending stability analysis of Zholkovskij *et al.* [22] for the prototypical case of concentric circular electrodes, and the stability criterion is extended to arbitrary two-dimensional geometries by conformal mapping. Experiments are performed for an aqueous CuSO$_4$ solution in a circular copper electrodeposition cell, confirming this instability.

The prototypical model for EOI-CE is a dilute, binary $z : z$ electrolyte of concentration (c_0) in an annular channel with an inner anode of radius R_1 and outer cathode of radius R_2 [Fig. 1(a)]. Geometrical curvature is controlled by the ratio $\chi = R_1/R_2 < 1$. For ion transport, there are two regions: the outer bulk electroneutral region valid in the segment $\chi < r < 1$ and the inner electric double layer region valid in the ε vicinity of the interfaces, where $\varepsilon = (dRT/4z^2F^2\pi c_0)^{1/2}/R_2$ is the dimensionless Debye length [6]. In the bulk electroneutral region, the governing equations are the dimensionless Nernst-Planck-Stokes equations [6]:

$$\bar{c}_t + \text{Pe}(\boldsymbol{v} \cdot \nabla)\bar{c} = \nabla \cdot (\nabla\bar{c} + \bar{c}\nabla\bar{\varphi}), \tag{1a}$$

$$\bar{c}_t + \text{Pe}(\boldsymbol{v} \cdot \nabla)\bar{c} = \nabla \cdot (\nabla\bar{c} - \bar{c}\nabla\bar{\varphi}), \tag{1b}$$

$$-\nabla\bar{p} + \Delta\bar{\boldsymbol{v}} = \frac{1}{\text{Sc}}\bar{\boldsymbol{v}}_t, \tag{1c}$$

$$\nabla \cdot \bar{\boldsymbol{v}} = 0, \qquad \bar{\boldsymbol{v}} = \bar{u}\boldsymbol{i}_r + \bar{w}\boldsymbol{i}_\theta, \tag{1d}$$

where $\bar{c} = c^+ = c^-$ is the ionic concentration scaled by c_0, $\bar{\varphi}$ the electric potential scaled by the thermal voltage, RT/zF, and $\bar{\boldsymbol{v}}$ is the fluid velocity scaled by $(RT/zF)^2(d/4\pi\eta R_2)$, where d is the dielectric constant and η the dynamic viscosity of the solution; for simplicity, the ionic diffusivities are assumed to be equal, $D_+ = D_- = D$; the solution is governed by the material Peclet number $\text{Pe} = (RT/zF)^2(d/4\pi\eta D)$ and the Schmidt number, $\text{Sc} = \nu/D$, since position is scaled to the outer radius R_2 and time to the diffusion time, R_2^2/D.

The dimensionless boundary conditions at each interface are

$$(\bar{c}_r - \bar{c}\varphi_r)|_{r=\chi,1} = 0, \quad \ln\bar{c} + \bar{\varphi}|_{r=\chi} = \ln p_1 + V, \tag{2a}$$

$$\ln\bar{c} + \bar{\varphi}|_{r=1} = \ln p_1, \quad \bar{u}|_{r=\chi,1} = 0, \quad \bar{w}|_{r=\chi,1} = w_s, \tag{2b}$$
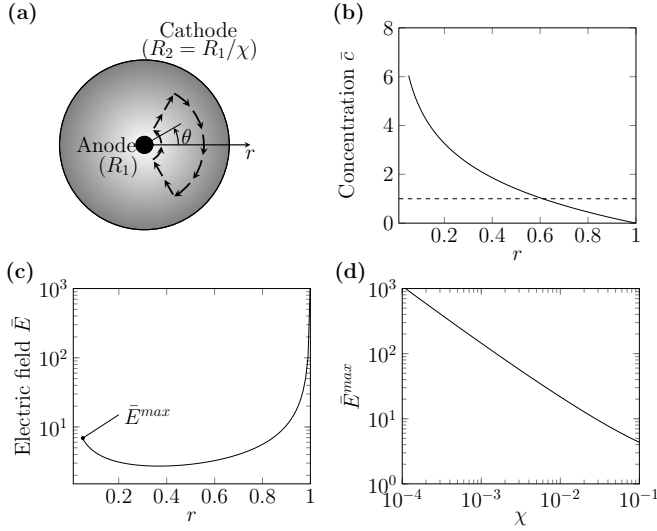
FIG. 1. (a) Sketch of the anode vortex near the inner anode in a circular channel. At limiting current, both the concentration enrichment (b) and an additional peak ($\bar{E}^p$) of electric field (c) appear near the inner anode. (d) $\bar{E}^p$ as a function of χ in a log-log scale, demonstrating the tendency of developing a singularity as $\chi \to 0$.

where p_1 is the fixed charge in the cation-selective interface, which could be a perm-selective membrane or electrode (as in our experiments below) and w_s is the equilibrium electro-osmotic slip from the electric double layer. The potential $\varphi = V$ at inner electrode $r = \chi$, and $\varphi = 0$ at outer electrode $r = 1$. Hereafter we assume $V > 0$ for the inner anode case to explore the electro-osmotic instability of concentration enrichment.

The complicated equations (1) and (2) admit an exact solution for the quiescent state of steady conduction with $\bar{v} = 0$ in any two-dimensional geometry [23]. For the circular geometry, the outer bulk electroneutral equations can be integrated to obtain the ionic fluxes [6,10,24]:

$$\frac{d\bar{c}}{dr} + \bar{c}\frac{d\bar{\varphi}}{dr} = -\frac{I}{2\pi r}, \quad \frac{d\bar{c}}{dr} - \bar{c}\frac{d\bar{\varphi}}{dr} = 0, \tag{3}$$

where I is the cation flux (equal to current density), scaled to the diffusion-limited current. The solution of Eq. (3) is

$$\bar{c}(r) = 1 - \frac{I}{4\pi}\left(\ln r + \frac{1}{2} + \frac{\chi^2 \ln \chi}{1 - \chi^2}\right). \tag{4}$$

Then the electric field is given by

$$\bar{E} = -\frac{d(\ln \bar{c})}{dr} \to -\frac{1}{r \ln r}, \quad \text{as } I \to 1. \tag{5}$$

According to Eq. (4), the ion concentration is enriched near the inner anode and depleted near the outer cathode [Fig. 1(b)]. However, in contrast to the parallel geometry [22], the electric field has two peaks [Fig. 1(c)]. One peak at $r = 1$ is related to concentration depletion near the outer cathode, common in the concentration polarization phenomenon. The other at $r = \chi$ of magnitude, $\bar{E}^{\max}(\chi) = -1/\chi \ln\chi$, is a special feature of the circular channel [Fig. 1(d)], which becomes singular in the limit of vanishing anode radius, $\chi \to 0$, and provides the driving force for instability.

To quantitatively investigate this possible electro-osmotic instability of concentration enrichment by identifying the instability growth rate (ω) dependent on the perturbation wave number (k), we perform the linear stability analysis of equations (1) and (2) at the limiting current, extending the
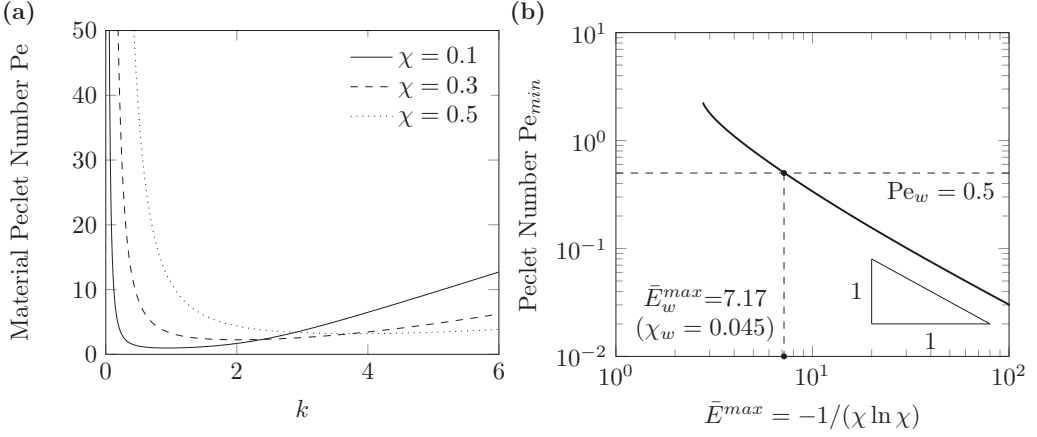
FIG. 2. Linear stability analysis. (a) The neutral stability curves versus dimensionless wave number k for various radius ratios χ, showing the critical material Peclet number Pe_{min} for each curve. (b) Nearly inverse dependence of Pe_{min} on the maximum electric field on the anode, $\bar{E}^{max} = -(\chi \ln \chi)^{-1}$. For aqueous electrolyte with $Pe_{aqu} = 0.5$, instability occurs for $\bar{E}^{max} > \bar{E}_w^{max} = 7.17$ or $\chi < \chi_w = 0.045$.

results of Ref. [22] to curved interfaces (see Supplemental Material [25] Note 1). In a circular channel, the equilibrium electro-osmotic slip velocity for the inner electric double layer valid in the ε vicinity of the interfaces is $w_s = [4 \ln 2 \frac{1}{r} \frac{\partial(\ln \bar{c})}{\partial \theta}]|_{r=\chi,1}$ at $r = \chi, 1$ (see Supplemental Material [25] Note 2).

The neutral stability curves for growth rate $\omega = 0$ [Fig. 2(a)] indicate a minimum material Pelect number Pe_{min} for various χ, above which the EOI-CE is possible. This $Pe_{min}(\chi)$ decreases dramatically with χ [Fig. 2(b)], and once $\chi < \chi_{cri}$, $Pe_{min} < Pe_{aqu}$ ($Pe_{aqu} \simeq 0.5$ is the typical material Peclet number of an aqueous electrolyte solution [22]).

Therefore, the electro-osmotic instability of concentration enrichment is possible in a circular channel ($\chi < \chi_{cri}$). Furthermore, the growth rate is always negative for $v|_{r=\chi} = 0$, $v|_{r=1} = w_s$, implying no instability at the outer cathode, but the instability can occur at the inner anode. In contrast to the planar-parallel case [22], the dimensionless inner radius χ provides another degree of freedom to control Pe_{min}, allowing its reduction by more than an order of magnitude, so that $Pe_{min} < Pe_{aqu}$ for $\chi < \chi_{cri}$. This opens the possibility of instability, even for an aqueous electrolyte.

For equal ionic diffusivities and perfectly perm-selective interface with infinite lateral conductivity, assumed in this Rapid Communication, the electrical body force alone cannot yield instability for a material Peclet number relevant for aqueous electrolytes [26–28]. Indeed, this force is negligible from scaling analysis, and has little effect on the neutral stability curves by stability analysis (see Supplemental Material [25] Note 3).

Linear stability of EOI-CE is dominated by the local physics of equilibrium electro-osmotic convection near the anode surface, so the stability criterion, expressed in terms of the local electric field, should hold for any locally smooth geometry, if the surface is not too highly curved. In particular, the most unstable wavelength should be smaller than the radius of curvature. For this regime in the circular geometry ($1/k \ll \chi$), the linear stability criterion plotted in Fig. 2(b) is well approximated by the inverse relation, $Pe_{min}/Pe_{aqu} < \bar{E}_w^{max}/\bar{E}^{max}$, where $Pe_{aqu} = 0.5$ and $\bar{E}_w^{max} = 7.17$.

This suggests a general stability criterion based on a bound for the dimensionless local electric field on the anode in the quiescent state,

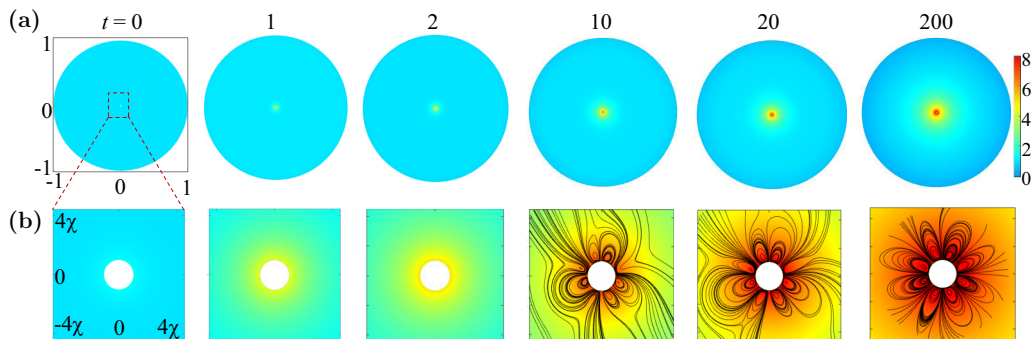$$\text{Stable if: } \bar{E}^{max} < \alpha/Pe, \tag{6}$$

FIG. 3. Numerical simulation. (a) Top panel for the concentration evolution. (b) Bottom panel for the magnified view around the inner anode, demonstrating the development of EOI and the formation of vortices indicated by the black streamlines in the concentration enrichment region. ($\chi = 1/120$, $V = 8$, $\varepsilon = 3 \times 10^{-4}$, $p_1 = 2$, and time scaled by $\chi^2 R_2^2/D$.)

where $\alpha \approx 14.34$. Using the general solution of the Nernst-Planck equations in two dimensions [23,29], $\bar{E}^{\mathrm{max}}$ can be derived for any anode geometry (see Supplemental Material [25] Note 4):

$$\bar{E}^{\mathrm{max}} = \max\left\{\frac{|f'(z)|\,I}{1+I}, \ \mathrm{Im} f(z) = 1\right\}, \tag{7}$$

where $w = f(z)$ is the conformal map from the electrolyte domain in the complex z plane to the strip, $|\mathrm{Im}\, w| < 1$, representing parallel-plate electrodes in the mathematical w plane. For the circular geometry (Fig. 1), which is defined by the conformal map, $f(z) = -i(1 - 2 \log z / \ln \chi)$, we recover the result above, $\bar{E}^{\mathrm{max}} = -1/(\chi \ \ln \chi)$, at the limiting current, $I = 1$.

In order to explore the nonlinear evolution of the instability, we perform a numerical simulation of the coupled Nernst-Planck-Poisson and Navier-Stokes equations [30–33] (see Supplemental Material [25] Note 5 and Video 1) for the prototypical circular geometry. The concentration evolution [Fig. 3(a)] shows the development of concentration depletion near the outer cathode and concentration enrichment near the inner anode ($\chi = 1/120 < \chi_{\mathrm{cri}}$). From Eq. (4), $c(\chi) \approx -2 \ln \chi \approx 10$ in the steady state is comparable with the concentration enrichment near the anode in the simulation. The magnified view of the concentration enrichment region around the inner anode [Fig. 3(b)] demonstrates the development of EOI and the formation of vortex indicated by the black streamlines. Moreover, at a large ratio such as $\chi = 1/10 > \chi_{\mathrm{cri}}$, the vortex disappears in the simulation, hence for EOI-CE a sufficient smaller χ is necessary, which is consistent with the linear stability analysis.
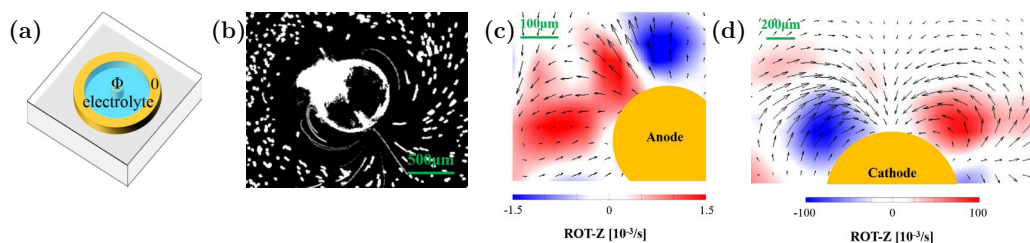

FIG. 4. Experimental observation of anode vortex in a circular channel. (a) The sketch of the electrochemical cell for a circular channel. (b) The observation of the anode vortex by the time-lapse imaging indicating the streamline ($\chi = 1/60$, $I = 5\ \mu A$). particle image velocimetry imaging of the flow field (c) near the inner anode ($\chi = 1/120$, $\Phi = 6$ V) and (d) near the inner cathode ($\chi = 1/120$, $\Phi = -6$ V).

TABLE I. Comparison between EOI-CE and NE-EOI in the aqueous electrolyte solution.

Type	Geometry	Current	Concentration	Mechanism	Size	Velocity	Vorticity
NE-EOI	Plane-parallel or circular	Overlimiting	Depletion region	Extended space charge	500 μm	10 μm/s	0.1 s^{-1}
EOI-CE	Circular with an inner anode	Limiting	Enrichment region	Enhanced electric field	200 μm	0.5 μm/s	0.001 s^{-1}

The electro-osmotic instability of concentration enrichment in the prototypical circular geometry is further verified by experiments. A circular channel embedded in a polydimenthylsiloxane device [Fig. 4(a)] is designed [24]; $H \approx 40$ μm for the channel height, $2R_2 = 24$ mm for the outer copper ring, and $2R_1 = 2.4$, 0.4, and 0.2 mm for the inner copper wire, corresponding to $\chi = 1/10$, $1/60$, and $1/120$. The aqueous CuSO$_4$ solution is 1 mM, and $\Phi = 6$ V (a Keithley 2450 Source Meter) for the inner anode. As expected, for $\chi = 1/10 > \chi_{cri}$, no instability is found in the region of concentration enrichment near the central anode. However, for $\chi < \chi_{cri}$, as predicted by the stability analysis and numerical simulations, the streamlines from 20-s time-lapse imaging [Fig. 4(b), $\chi = 1/60$] (fluorescent microscope, Zeiss, Axio Zoom V16) [24] are clearly observed near the central anode, evidently demonstrating the existence of the EOI-CE. Furthermore, by employing particle image velocity [Fig. 4(c), $\chi = 1/120$], this anode vortex is weak with velocity about 1 μm/s.

We also compared our described electro-osmotic instability of concentration enrichment with the NE-EOI for the inner cathode [Fig. 4(d)] in the circular channel via experiments (Table I) and simulations (see Supplemental Material [25] Note 6). Experimentally, the anode vortex is much weaker with its vorticity about two orders of magnitude lower than the cathodic one, and its velocity about 1 μm/s or lower. Consequently, as opposed to the cathode vortex in the concentration depletion region enhancing the ion transport and sustaining the overlimiting conductance, the current is not affected much by the presence of an anode vortex which is confirmed in simulations (see Supplemental Material [25] Note 7).

As noted previously for a plane-parallel geometry [22], theoretically the equilibrium EOI instability is feasible though only for an unrealistically high material Peclet number (Pe > Pe$_{min}$). Indeed, the simulations in this planar geometry (see Supplemental Material [25] Video 2 for Pe = 50, $V = 4$) confirm that the EOI occurs in the concentration enrichment region near the anode side, not the concentration depleted near the cathode side. Furthermore, this positive (negative) feedback near the concentration enrichment (depletion) interface is clearly unraveled by an illustration of the concentration and potential perturbation from a seeding vortex upon a basic quiescent concentration polarization steady state (see Supplemental Material [25] Note 8).

The prerequisite for this equilibrium electro-osmotic instability is exclusively in the enriched region, i.e., as opposed to that addressed by Rubinstein and Zaltzman [6,19], this instability is initiated at the enriched interface (anode), rather than at the depleted one (cathode). Also the high electric field at the inner anode due to line charge singularity eliminates the limitation of unrealistically high Pe observed by Zholkovsky *et al.* for planar geometry [22], hence allowing the experimental observation of this instability in an aqueous solution here.

This reported instability has practical implications to enhance membrane processes, such as reverse osmosis, by convective mixing of the concentrated brine layer, stimulated by needlelike curved electrodes driving EOI-CE. For example, cylindrical hollow membrane fiber is a central element of desalination by reverse osmosis [34] and energy conversion by pressure-retarded osmosis [35] employing salinity variation, while salt accumulation at the membrane is the major limitation of these processes. Hence, introducing the anode into the fiber and reducing the salt accumulation near the anode fiber through instability could be a major remedy for this limitation.

ACKNOWLEDGMENTS

[1] R. F. Probstein, *Physicochemical Hydrodynamics* (Wiley, New York, 2003).

[2] M. A. Shannon, P. W. Bohn, M. Elimelech, J. G. Georgiadis, B. J. Marinas, and A. M. Mayes, Science and technology for water purification in the coming decades, Nature (London) **452**, 301 (2008).

[3] V. V. Nikonenko, A. V. Kovalenko, M. Urtenov, N. D. Pismenskaya, J. Han, P. Sistat, and G. Pourcelly, Desalination at overlimiting currents: State-of-the-art and perspectives, Desalination **342**, 85 (2014).

[4] S. S. Dukhin, Electrokinetic phenomena of the second kind and their applications, Adv. Colloid Interface Sci. **35**, 173 (1991).

[5] I. Rubinstein and B. Zaltzman, Electro-osmotically induced convection at a permselective membrane, Phys. Rev. E **62**, 2238 (2000).

[6] B. Zaltzman and I. Rubinstein, Electro-osmotic slip and electroconvective instability, J. Fluid Mech. **579**, 173 (2007).

[7] S. J. Kim, Y. C. Wang, J. H. Lee, H. Jang, and J. Han, Concentration Polarization and Nonlinear Electrokinetic Flow Near a Nanofluidic Channel,, Phys. Rev. Lett. **99**, 044501 (2007).

[8] S. Rubinstein, G. Manukyan, A. D. Staicu, I. Rubinstein, B. Zaltzman, R. G. H. Lammertink, F. G. Mugele, and M. Wessling, Direct Observation of a Nonequilibrium Electro-Osmotic Instability, Phys. Rev. Lett. **101**, 236101 (2008).

[9] G. Yossifon and H.-C. Chang, Selection of Nonequilibrium Overlimiting Currents: Universal Depletion Layer Formation Dynamics and Vortex Instability, Phys. Rev. Lett. **101**, 254501 (2008).

[10] E. V. Dydek, B. Zaltzman, I. Rubinstein, D. S. Deng, A. Mani, and M. Z. Bazant, Overlimiting Current in a Microchannel, Phys. Rev. Lett. **107**, 118301 (2011).

[11] A. Yaroshchuk, E. Zholkovskiy, S. Pogodin, and V. A. Baulin, Coupled concentration polarization and electroosmotic circulation near micro/nanointerfaces: Taylor-Aris model of hydrodynamic dispersion and limits of its applicability, Langmuir **27**, 11710 (2011).

[12] C. P. Nielsen and H. Bruus, Concentration polarization, surface currents, and bulk advection in a microchannel, Phys. Rev. E **90**, 043020 (2014).

[13] S. Nam, I. Cho, J. Heo, G. Lim, M. Z. Bazant, D. J. Moon, G. Y. Sung, and S. J. Kim, Experimental Verification of Overlimiting Current by Surface Conduction and Electro-Osmotic Flow in Microchannels, Phys. Rev. Lett. **114**, 114501 (2015).

[14] D. S. Deng, E. V. Dydek, J. Han, S. Schlumpberger, A. Mani, B. Zaltzman, and M. Z. Bazant, Overlimiting current and shock electrodialysis in porous media, Langmuir **29**, 16167 (2013).

[15] S. Alizadeh, M. Z. Bazant, and A. Mani, Impact of network heterogeneity on electrokinetic transport in porous media, J. Colloid Interface Sci. **553**, 451 (2019).

[16] D. S. Deng, W. Aouad, W. A. Braff, S. Schlumpberger, M. E. Suss, and M. Z. Bazant, Water purification by shock electrodialysis: Deionization, filtration, separation, and disinfection, Desalination **357**, 77 (2015).

[17] S. Schlumpberger, N. B. Lu, M. E. Suss, and M. Z. Bazant, Scalable and continuous water deionization by shock electrodialysis, Environ. Sci. Technol. Lett. **2**, 367 (2015).

[18] K. M. Conforti and M. Z. Bazant, Continuous ion-selective separations by shock electrodialysis, AIChE J. **66**, e16751 (2020).

[19] I. Rubinstein and B. Zaltzman, Equilibrium Electroconvective Instability, Phys. Rev. Lett. **114**, 114502 (2015).

[20] R. Abu-Rjal, I. Rubinstein, and B. Zaltzman, Driving factors of electro-convective instability in concentration polarization, Phys. Rev. Fluids **1**, 023601 (2016).

[21] I. Rubinstein, Electroconvection at an electrically inhomogeneous permselective interface, Phys. Fluids **3**, 2301 (1991).

[22] E. K. Zholkovskij, M. A. Vorotyntsev, and E. Staude, Electrokinetic instability of solution in a plane-parallel electrochemical cell, J. Colloid Interface Sci. **181**, 28 (1996).

[23] M. Z. Bazant, Conformal mapping of some non-harmonic functions in transport theory, Proc. R. Soc. London, Ser. A **460**, 1433 (2004).

[24] Z. B. Gu, B. R. Xu, P. Huo, S. Rubinstein, M. Z. Bazant, and D. S. Deng, Deionization shock driven by electroconvection in a circular channel, Phys. Rev. Fluids **4**, 113701 (2019).

[25] See Supplemental Material at http://link.aps.org/supplemental/10.1103/PhysRevFluids.5.091701 for details on the theory and simulation, videos 1 and 2, which includes Refs. [36–39].

[26] J. C. Baygents and F. Baldessari, Electrohydrodynamic instability in a thin fluid layer with an electrical conductivity gradient, Phys. Fluids **10**, 301 (1998).

[27] R. S. Aleksandrov, A. P. Grigin, and A. D. Davydov, Numerical simulation of Rayleigh-Bènard instability in solutions containing ions of three types, Russ. J. Electrochem. **38**, 616 (2002).

[28] B. D. Storey, B. Zaltzman, and I. Rubinstein, Bulk electroconvective instability at high Péclet numbers, Phys. Rev. E **76**, 041501 (2007).

[29] M. Z. Bazant, J. Choi, and B. Davidovitch, Dynamics of Conformal Maps for a Class of Non-Laplacian Growth Phenomena, Phys. Rev. Lett. **91**, 045503 (2003).

[30] C. L. Druzgalski, M. B. Andersen, and A. Mani, Direct numerical simulation of electroconvective instability and hydrodynamic chaos near an ion-selective surface, Phys. Fluids **25**, 110804 (2013).

[31] E. Karatay, C. L. Druzgalski, and A. Mani, Simulation of chaotic electrokinetic transport: Performance of commercial software versus custom-built direct numerical simulation codes, J. Colloid Interface Sci. **446**, 67 (2015).

[32] P. Shi and W. Liu, Length-dependent instability of shear electroconvective flow : From electroconvective instability to Rayleigh- Bénard instability, J. Appl. Phys. **124**, 204304 (2018).

[33] W. Liu, Y. Zhou, and P. Shi, Shear electroconvective instability in electrodialysis channel under extreme depletion and its scaling laws, Phys. Rev. E **101**, 043105 (2020).

[34] L. F Greenlee, D. F. Lawler, B. D. Freeman, B. Marrot, and P. Moulin, Reverse osmosis desalination: Water sources, technology, and today's challenges, Water Research **43**, 2317 (2009).

[35] A. Achilli, T. Y. Cath, and A. E. Childress, Power generation with pressure retarded osmosis: An experimental and theoretical investigation, J. Membr. Sci. **343**, 42 (2009).

[36] S. S. Dukhin and B. V. Derjaguin, *Electrophoresis* (Nauka (Russian), Moscow, 1976).

[37] J. R. Philip and R. A. Wooding, Solution of the poisson-boltzmann equation about a cylindrical particle, J. Chem. Phys. **52**, 953 (1970).

[38] J. Parlange, Note on the poisson-boltzmann equation, J. Chem. Phys. **57**, 376 (1972).

[39] R. E. Rice and F. H. Horne, Analytical solution of the linearized poisson-boltzmann equation in cylindrical coordinates, J. Chem. Phys. **75**, 5582 (1981).